# $CO_2$ semiannual oscillation in the middle troposphere and at the surface

Xun Jiang,[1] Moustafa T. Chahine,[2] Qinbin Li,[3] Maochang Liang,[4] Edward T. Olsen,[2] Luke L. Chen,[2] Jingqian Wang,[1] and Yuk L. Yung[5]

Received 24 May 2011; revised 22 April 2012; accepted 26 June 2012; published 28 July 2012.

[1] Using in situ measurements, we find a semiannual oscillation (SAO) in the midtropospheric and surface $CO_2$. Chemistry transport models (2-D Caltech/JPL model, 3-D GEOS-Chem, and 3-D MOZART-2) are used to investigate possible sources for the SAO signal in the midtropospheric and surface $CO_2$. From model sensitivity studies, it is revealed that the SAO signal in the midtropospheric $CO_2$ originates mainly from surface $CO_2$ with a small contribution from transport fields. It is also found that the source for the SAO signal in surface $CO_2$ is mostly related to the $CO_2$ exchange between the biosphere and the atmosphere. By comparing model $CO_2$ with in situ $CO_2$ measurements at the surface, we find that models are able to capture both annual and semiannual cycles well at the surface. Model simulations of the annual and semiannual cycles of $CO_2$ in the tropical middle troposphere agree reasonably well with aircraft measurements.

**Citation:** Jiang, X., M. T. Chahine, Q. Li, M. Liang, E. T. Olsen, L. L. Chen, J. Wang, and Y. L. Yung (2012), $CO_2$ semiannual oscillation in the middle troposphere and at the surface, *Global Biogeochem. Cycles*, *26*, GB3006, doi:10.1029/2011GB004118.

## 1. Introduction

[2] Atmospheric $CO_2$ has a trend of ~2 ppm/yr based on measurements from Mauna Loa covering from 1958 to 1994 [*Keeling et al.*, 1995]. The increasing atmospheric $CO_2$ has a significant impact on the global climate system [*Dickinson and Cicerone*, 1986]. Superimposed upon this trend is an annual cycle resulting from the uptake and release of $CO_2$ by vegetation whose amplitude is greatest in the northern hemisphere (NH). Using $CO_2$ measurements at Mauna Loa, *Buermann et al.* [2007] found that variations of $CO_2$ seasonal cycle amplitudes are closely related to carbon sequestration in the biosphere, and are influenced by precipitation and circulation. In addition to the trend and annual cycle, atmospheric $CO_2$ also demonstrates intraseasonal and interannual variabilities.

[3] El Niño is the most important tropical interannual variability that can influence the $CO_2$ concentrations. During El Niño (La Niña) events, the atmospheric $CO_2$ growth rate increases (decreases) at tropical surface stations [*Keeling et al.*, 1995; *Jones et al.*, 2001; *Nevison et al.*, 2008]. Using midtropospheric $CO_2$ data from the Atmospheric Infrared Sounder, *Jiang et al.* [2010] found that El Niño can influence the midtropospheric $CO_2$ concentrations. Midtropospheric $CO_2$ is enhanced in the central Pacific Ocean and diminished in the western Pacific Ocean during El Niño [*Jiang et al.*, 2010]. In the high latitudes, midtropospheric $CO_2$ concentration can be influenced by the strength of the polar vortex. Polar midtropospheric $CO_2$ is reduced (enhanced) when the polar vortex is strong (weak) [*Jiang et al.*, 2010]. Recently, *Li et al.* [2010] demonstrated that midtropospheric $CO_2$ concentrations are also modulated by the Madden-Julian oscillation.

[4] In this paper, we will focus on investigating the intraseasonal variability of midtropospheric $CO_2$, especially on the $CO_2$ semiannual oscillation (SAO) and its possible causes. This work will yield a quantitative study of how SAO influences the midtropospheric $CO_2$. It also offers an opportunity to investigate the possible cause for the SAO signal in the midtropospheric $CO_2$.

## 2. Data and Models

[5] In this paper, we use aircraft $CO_2$ from *Matsueda et al.* [2002], which are incorporated into the Comprehensive Observation Network for Trace gases by AIrLiner (CONTRAIL). Aircraft $CO_2$ from *Matsueda et al.* [2002] are measured at 8–13 km biweekly since April 1993 to the present over the western Pacific from Australia to Japan. The latitudinal coverage is approximately from 25°S to 35°N. The longitudinal coverage is from 135°E to 150°E. We also use surface $CO_2$ flask measurements from NOAA ESRL network [*Tans et al.* 1998; *Earth System Research Laboratory*

[1]Department of Earth and Atmospheric Sciences, University of Houston, Houston, Texas, USA.
[2]Science Division, Jet Propulsion Laboratory, California Institute of Technology, Pasadena, California, USA.
[3]Department of Atmospheric and Oceanic Sciences, University of California, Los Angeles, California, USA.
[4]Research Center for Environmental Changes, Academia Sinica, Taipei, Taiwan.
[5]Division of Geological and Planetary Sciences, California Institute of Technology, Pasadena, California, USA.

Corresponding author: X. Jiang, Department of Earth and Atmospheric Sciences, University of Houston, Houston, TX 77004, USA. (xjiang4@mail.uh.edu)


0886-6236/12/2011GB004118

(ESRL), 2007]. Site information for NOAA surface $CO_2$ is available at http://www.esrl.noaa.gov/gmd/dv/site/site_table.html.

[6] To investigate the possible causes of the semiannual oscillation of midtropospheric and surface $CO_2$, we use three different chemistry transport models. These models are the Caltech/JPL 2-D chemistry transport model (CTM) [*Shia et al.*, 2006], 3-D GEOS-Chem [*Suntharalingam et al.*, 2004], and 3-D MOZART-2 [*Horowitz et al.*, 2003]. The 2-D CTM has 18 latitudes, equally spaced from pole to pole. It has 40 vertical layers, equally spaced in log scale of pressure from the surface to the upper boundary at 0.01 hPa. Transport in the model is by the stream function and the horizontal and vertical diffusivities taken from *Jiang et al.* [2004]. The stream function is derived from the National Center for Climate Prediction (NCEP) Reanalysis 2 data [*Jiang et al.*, 2004]. An important feature of the 2-D CTM is its ability to reproduce the age of air in the stratosphere [*Morgan et al.*, 2004].

[7] GEOS-Chem (v7.3.3) is driven by the Goddard Earth Observing System (GEOS-4) assimilated meteorological data from the NASA Global Modeling Assimilation Office (GMAO). Spatial resolution for GEOS-Chem is 2° (latitude) × 2.5° (longitude). There are 30 levels in the vertical from the surface to about 0.01 hPa (~70 km). Advection is computed every 15 min with a flux form semi-Lagrangian method [*Lin and Rood*, 1996]. Moist convection is computed using the GEOS convective, entrainment, and detrainment mass fluxes described by *Allen et al.* [1996a, 1996b]. The physics in the GEOS-4 analysis system is adopted from the National Center for Atmospheric Research (NCAR) Community Climate Model, Version 3 (CCM3) and Whole Atmosphere Community Climate Model (WACCM) with important modifications to make it suitable for data assimilation [*Bloom et al.*, 2005].

[8] MOZART-2 is driven by the meteorological inputs every 6 h from the NCEP Reanalysis 1 [*Kalnay et al.*, 1996]. Advection is computed every 20 min with a flux form semi-Lagrangian method [*Lin and Rood*, 1996]. The horizontal resolution is 2.8° (latitude) × 2.8° (longitude) with 28 vertical levels extending up to approximately 40 km altitude [*Horowitz et al.*, 2003]. MOZART-2 is built on the framework of the Model of Atmospheric Transport and Chemistry (MATCH). MATCH includes representations of advection, convective transport, boundary layer mixing, and wet and dry deposition.

[9] Surface emissions and vertical transport in CTMs are both crucial for $CO_2$ simulation in the free troposphere. We will use two different boundary conditions to investigate how boundary conditions affect the midtropospheric $CO_2$. The GLOBALVIEW-$CO_2$ mixing ratio data [*Tans et al.* 1998; *ESRL*, 2007] are used as the lower boundary condition for the Caltech/JPL CTM, GEOS-Chem, and MOZART-2. For convenience, we refer to this hereforth as the GLOBALVIEW-$CO_2$ boundary condition [*Jiang et al.*, 2008]. Since the GLOBALVIEW-$CO_2$ data are limited in space, especially over the oceans, we used the GLOBALVIEW-$CO_2$ to rescale the monthly mean $CO_2$ mixing ratios at the surface for the GLOBALVIEW-$CO_2$ boundary condition. First, we use seasonal varying $CO_2$ source and sink flux boundary condition to drive the model. We also interpolate monthly mean GLOBALVIEW-$CO_2$ measurements to the model resolution. Then, we rescale the zonal mean $CO_2$ mixing ratio in the boundary by the monthly mean GLOBALVIEW-$CO_2$ measurements for each month and for each latitudinal band. The monthly mean GLOBALVIEW-$CO_2$ flask data are close to the colocated GLOBALVIEW-$CO_2$ boundary condition.

[10] We will also use prescribed $CO_2$ sources and sinks as the boundary condition for GEOS-Chem and MOZART-2. The exchange of $CO_2$ between the terrestrial biosphere and atmosphere is based on net primary productivity and respiration fluxes from the Carnegie-Ames-Stanford (CASA) ecosystem model [*Randerson et al.*, 1997]. Monthly mean biospheric $CO_2$ fluxes from 2000 to 2004 are used in the models, which includes interannual variability as that used in *Feng et al.* [2011]. Air-sea exchange of $CO_2$ is taken from *Takahashi et al.* [1997], which is an annual mean ocean $CO_2$ flux. Estimates of fossil fuel emissions are from G. Marland et al. (Global, Regional, and National Fossil-Fuel $CO_2$ Emissions, 2007, http://cdiac.ornl.gov/trends/emis/overview_2007.html), which is also an annual mean $CO_2$ flux. Monthly mean biomass burning emissions of $CO_2$ are based on *Duncan et al.* [2003]. Since there is an unbalanced $CO_2$ budget associated with the prescribed source and sink boundary condition [*Suntharalingam et al.*, 2003, 2004], we regress surface $CO_2$ mixing ratio in the GEOS-Chem restart file against the GLOBALVIEW-$CO_2$ surface flask measurements. As a result, the unbalanced $CO_2$ budget is resolved to some degree [*Jiang et al.*, 2008]. Discrepancies between the model $CO_2$ simulations (driven by the same meteorological fields) with the above mentioned two boundary conditions would help identify potential issues with the surface sources and/or sinks on simulating $CO_2$ annual and semiannual cycles.

## 3. Results

[11] Figure 1 presents a comparison between Matsueda's aircraft $CO_2$ (red dots) and model $CO_2$ mixing ratios averaged between 9 km and 13 km (solid lines) from 2000 to 2004. Figures 1a–1f show 25°S, 15°S, 5°S, 5°N, 15°N, and 25°N, respectively. Different color lines are for different model simulations. There are two GEOS-Chem model outputs. One is forced by the GLOBALVIEW-$CO_2$ boundary condition (green line). The other is forced by the prescribed $CO_2$ sources and sinks boundary condition (orange line). GEOS-Chem $CO_2$ forced by the prescribed $CO_2$ source/sink boundary condition (orange line) have higher $CO_2$ concentrations in the summer seasons than that forced by GLOBALVIEW-$CO_2$ boundary condition (green line). It suggests that there might be a missing sink in the prescribed $CO_2$ source/sink boundary condition in the summer season. The purple line is $CO_2$ from Caltech 2D model. The blue line is $CO_2$ from MOZART2 forced by NCEP1 meteorology. The model results match the high-precision aircraft measurements of $CO_2$ in the middle troposphere remarkably well. Seasonal cycle and trend for $CO_2$ are simulated well by different models. The amplitude of $CO_2$ seasonal cycle increases with latitudes, with larger seasonal cycle in the northern hemisphere compared with that in the southern hemisphere. In addition to the annual cycle, there is a

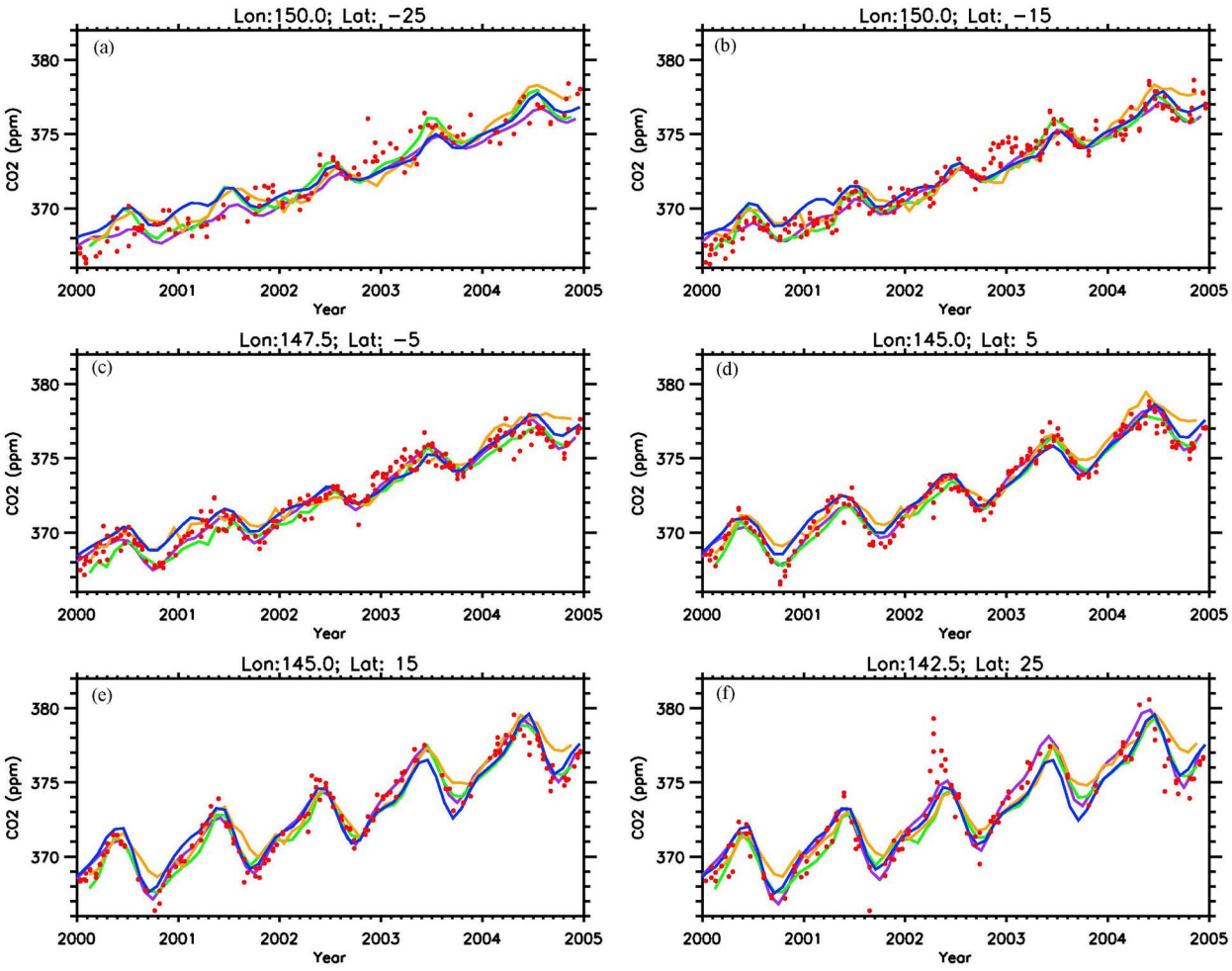


**Figure 1.** (a–f) Aircraft observations between 9 km and 13 km (red dots) [*Matsueda et al.*, 2002] and model $CO_2$ mixing ratios (color lines). The $CO_2$ mixing ratios from the GEOS-Chem model forced by the GLOBALVIEW-$CO_2$ boundary condition and prescribed $CO_2$ source/sink boundary condition are shown by the green and orange lines, respectively. The $CO_2$ mixing ratios from the Caltech/JPL 2-D model forced by NCEP2 and GLOBALVIEW-$CO_2$ BC are shown by the purple line. The $CO_2$ mixing ratios from MOZART-2 forced by NCEP1 and GLOBALVIEW-$CO_2$ BC are shown by the blue line.

6 month signal appearing in the $CO_2$ from both aircraft and model simulations. To investigate the 6 month signal in more detail, power spectral analysis is applied to the detrended $CO_2$ from aircraft and model simulations. Linear trends have been removed from $CO_2$ time series. Power spectra for the detrended $CO_2$ are shown in Figure 2. In addition to the spectral peak at 12 months, there are 6 month signals appearing in the power spectra of Matsueda's $CO_2$ and model $CO_2$.

[12] To investigate the causes of the semiannual oscillations in the midtropospheric $CO_2$, we first apply sensitivity studies to the 2-D Caltech/JPL chemistry and transport model. Averaged $CO_2$ at 9–13 km forced by the GLOBALVIEW-$CO_2$ boundary condition and NCEP2 meteorology is shown by the solid line in Figure 3. To investigate the annual cycle and semiannual cycle amplitudes in the midtropospheric $CO_2$, we fit the data by a series of Legendre polynomials and harmonic functions [*Jiang et al.*, 2008]. We use the sum of the first, second, and third Legendre polynomials to remove the trend from the data. The harmonic functions represent annual and semiannual cycles. Annual cycle, calculated by $e \cos(2\pi t) + f \sin(2\pi t)$, is shown in Figure 3b, where $e$ and $f$ are the amplitudes of the annual cycle. The amplitude for the annual cycle of 2-D model $CO_2$ at 25°N is about 2.3 ppm. The semiannual cycle, calculated by $g \cos(4\pi t) + h \sin(4\pi t)$, is shown in Figure 3c, where $g$ and $h$ are the amplitudes of the semiannual cycle. The amplitude for the semiannual cycle of 2-D model $CO_2$ at 25°N is about 0.8 ppm.

[13] In a sensitivity test, we remove the annual and semiannual oscillations from surface $CO_2$ and use linear trends as the boundary condition at the model surface. As such, there is no semiannual cycle and annual cycle source originating from surface in this model run. This results in the reduction of the amplitude of semiannual cycle for midtropospheric $CO_2$ to 0.09 ppm (black dotted line in Figure 3c), which is

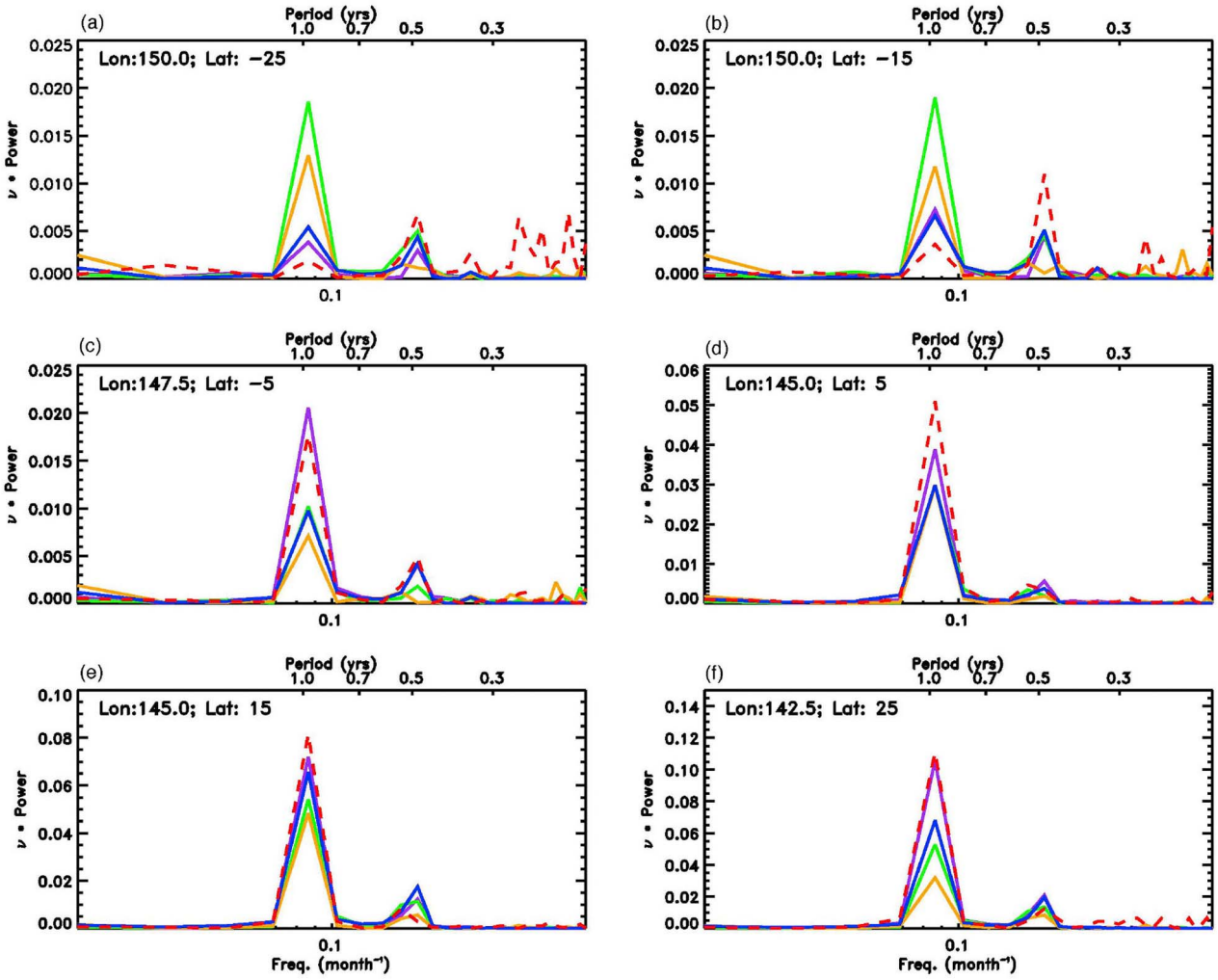


**Figure 2.** Power spectra for aircraft and model $CO_2$ time series. Red dashed line is the power spectra for the *Matsueda et al.* [2002] data. Colors for solid lines are the same as in Figure 1.

about 11% of the total amplitude of the semiannual oscillation in the midtropospheric $CO_2$. It clearly suggests that the dominant cause of the semiannual cycle in the middle troposphere is from the surface sources. Weak semiannual and annual cycles in the midtropospheric $CO_2$ shown by black dotted lines in Figures 3b and 3c originate from transport fields. The phase of the $CO_2$ seasonal cycle due to the transport (black dotted line in Figure 3b) is shifted relative to that forced by the GLOBALVIEW-$CO_2$ boundary condition and NCEP2 reanalysis meteorology field (black solid line in Figure 3b). The $CO_2$ seasonal signal due to the transport (black dotted line in Figure 3b) is related to the strength of the vertical velocity in the 2D CTM. The vertical velocity is stronger in the summer season and weaker in the winter season. More $CO_2$ can be lifted to the middle troposphere during the summer than in the winter season. Thus the midtropospheric $CO_2$ (black dotted line in Figure 3b) reaches maximum value in the summer season at 25°N. Although the vertical velocity peaks in summer, the $CO_2$ seasonal cycle (forced by the GLOBALVIEW-$CO_2$ boundary condition and NCEP2 reanalysis meteorology field; black solid line in Figure 3b) reaches maximum in April as a result of summertime drawdown by the biosphere. In another sensitivity test, we force the model with linear $CO_2$ trend boundary condition and climatological transport fields. Climatological transport fields are the average of the transport fields from 2000 to 2004. There is no semiannual oscillation originating from either the surface or the transport fields. As a result, the semiannual oscillation disappears in midtropospheric $CO_2$ as shown by the black dashed line in Figure 3c.

[14] To further reveal how the surface annual cycle and semiannual cycle relate to the semiannual oscillation in the midtropospheric $CO_2$, we decompose the net exchange between the biosphere and atmosphere (NEP) into the annual cycle and the semiannual cycle using the multiple regression method. Then, we use the combined $CO_2$ linear trend and annual cycle from the NEP as the boundary condition for the model. Result from this sensitivity study is shown by the green dotted line in Figure 3. We also use combined $CO_2$ linear trend and semiannual cycle from NEP as the boundary condition for the model, and result is shown

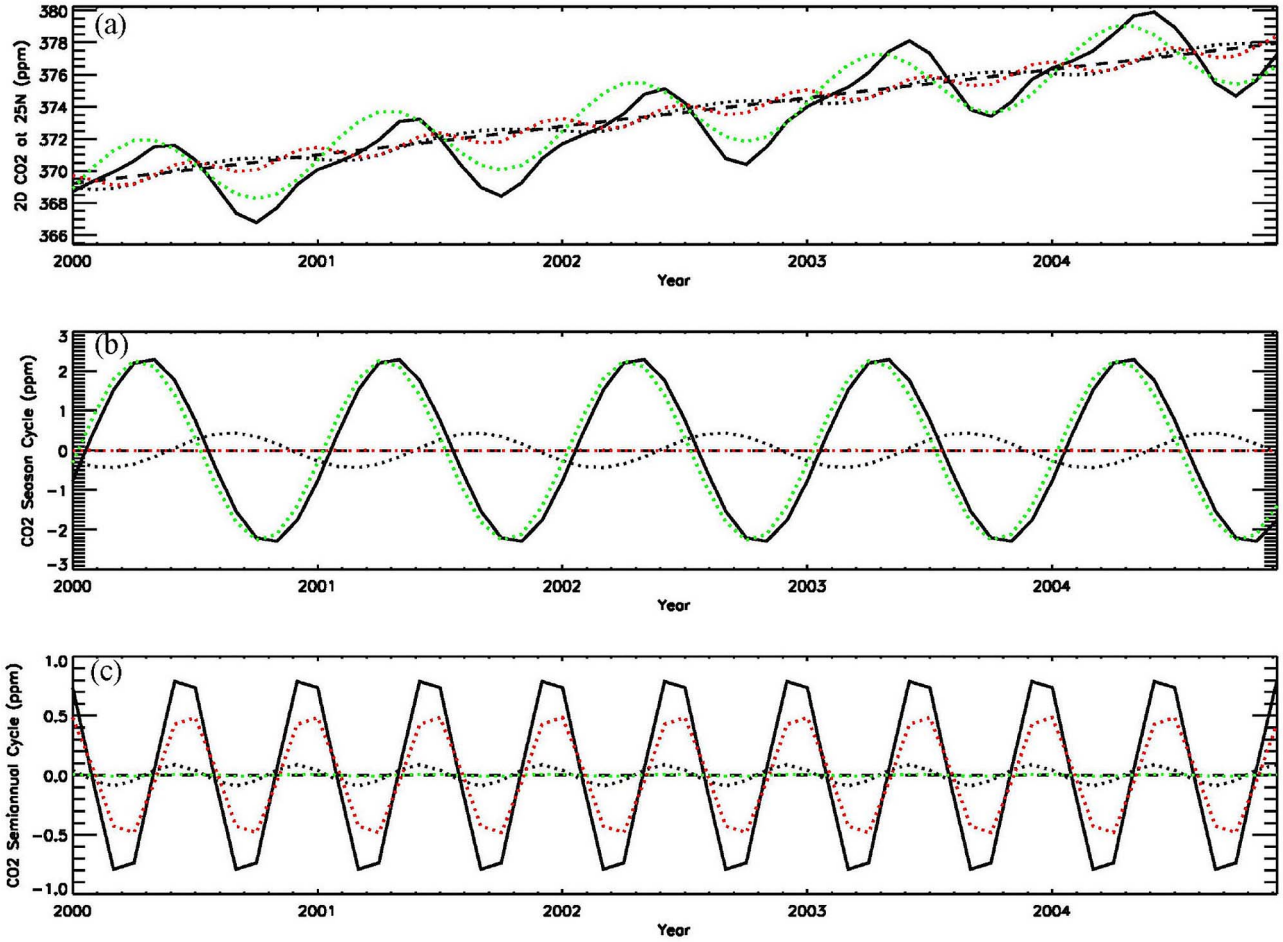


**Figure 3.** (a) Caltech/JPL 2-D model $CO_2$ at 25°N. (b) Seasonal cycle of model $CO_2$ at 25°N. (c) Semiannual cycle of model $CO_2$ at 25°N. Model $CO_2$ forced by the GLOBALVIEW-$CO_2$ boundary condition and NCEP2 reanalysis meteorology field are shown by the black solid line. Model $CO_2$ forced by the linear $CO_2$ trend boundary condition and NCEP2 reanalysis meteorology are shown by the black dotted line. Model $CO_2$ forced by the linear $CO_2$ trend boundary condition and climatology transport field are shown by the black dashed line. Model $CO_2$ forced by the combined linear $CO_2$ trend and annual cycle boundary condition and climatology transport field are shown by the green dotted line. Model $CO_2$ forced by the combined linear $CO_2$ trend and semiannual cycle boundary condition and climatology transport field are shown by the red dotted line. Units are ppm.

by the red dotted line in Figure 3. As shown in Figure 3, the semiannual oscillation signal in the midtropospheric $CO_2$ is mainly from the surface semiannual cycle instead of the surface annual cycle. From Figure 3c, we also find that the NEP is the major contribution to the SAO signal in the midtropospheric $CO_2$ and counts about 60% of the total SAO signal. In addition to the contribution from transport and the biosphere, $CO_2$ fluxes from biomass burning and exchange with the ocean can also contribute to the SAO signal in the middle troposphere. When we have better ocean $CO_2$ surface emissions in the future, we can decompose the contributions to the SAO signal into different components in a future paper.

[15] Annual and semiannual oscillations in surface $CO_2$ are also examined. Similar spectral analysis is applied to the GLOBALVIEW-$CO_2$ and GEOS-Chem model $CO_2$ at the surface. In addition to the annual cycle, semiannual oscillation signals are also present in the surface $CO_2$ from GLOBALVIEW-$CO_2$ and model $CO_2$. To compare the annual cycle and semiannual cycle amplitudes in surface $CO_2$ from observations and model results, we calculate the annual cycle amplitude ($\sqrt{e^2+f^2}$) and semiannual cycle amplitude ($\sqrt{g^2+h^2}$) for surface $CO_2$ from GLOBALVIEW network and GEOS-Chem model output. Results are shown in Figure 4. The amplitudes for annual and semiannual cycles from GEOS-Chem $CO_2$ are very close to those from GLOBALVIEW-$CO_2$ at the surface. The amplitudes of annual and semiannual cycles are larger in the northern hemisphere compared with those in the southern hemisphere. The maximum amplitude for the annual cycle of surface $CO_2$ is about ~10 ppm. The maximum amplitude is about ~3.5 ppm for the semiannual cycle of surface $CO_2$.

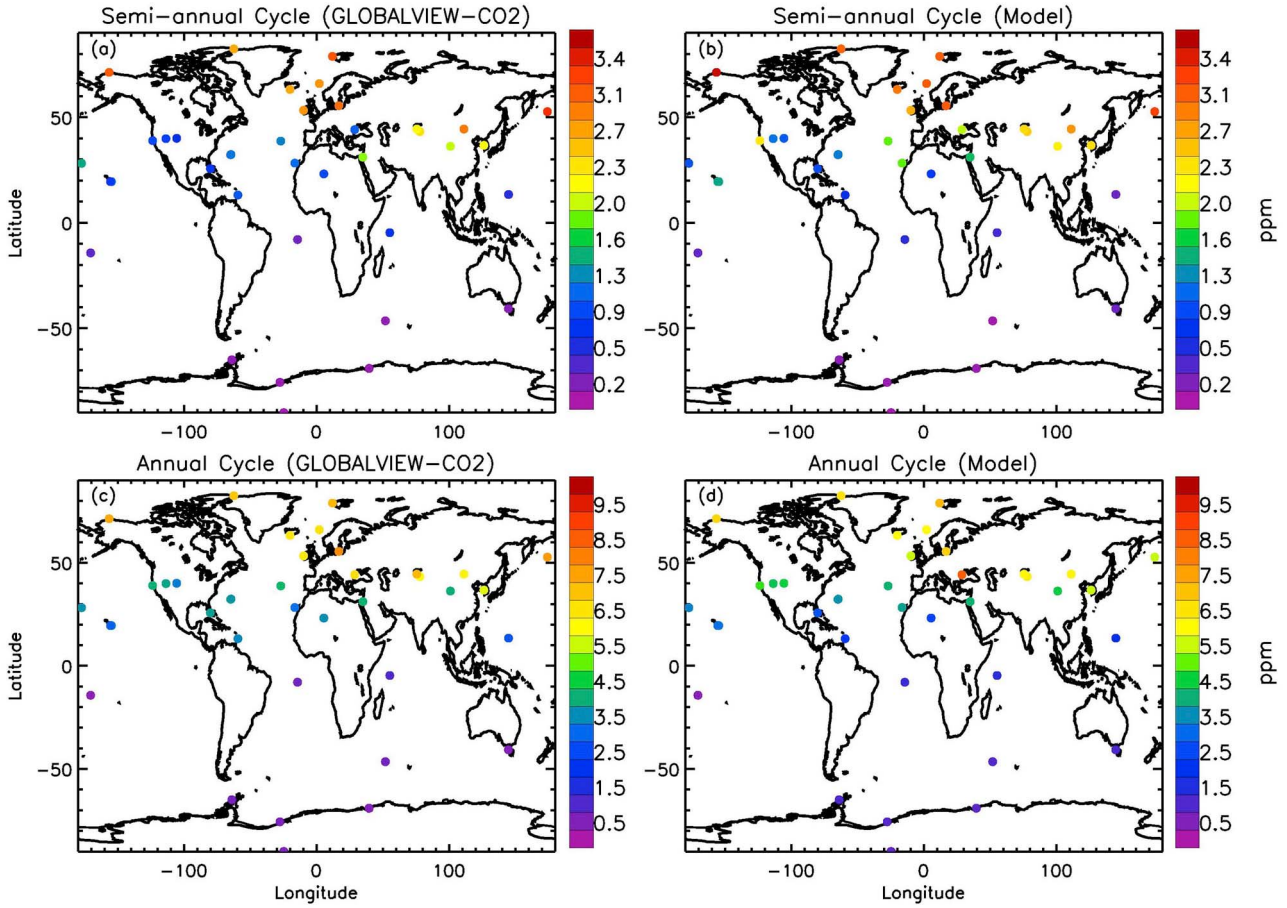


**Figure 4.** (a) Semiannual oscillation amplitude from GLOBALVIEW-$CO_2$ measurement. (b) Semiannual oscillation amplitude from GEOS-Chem model $CO_2$. (c) Annual cycle amplitude from GLOBALVIEW-$CO_2$ measurement. (d) Annual cycle amplitude from GEOS-Chem model $CO_2$. Units are ppm.

Scatterplots of the observed and model simulated amplitudes for semiannual cycle and annual cycle of surface $CO_2$ are shown in Figure 5. As shown in Figure 5, the GEOS-Chem model seems to overestimate the semiannual oscillation amplitudes at some stations. This might relate to the relatively coarse spatial resolution in the model. The latitudinal distributions of the amplitudes for the semiannual and annual cycles are shown in Figure 6. The amplitude increases with

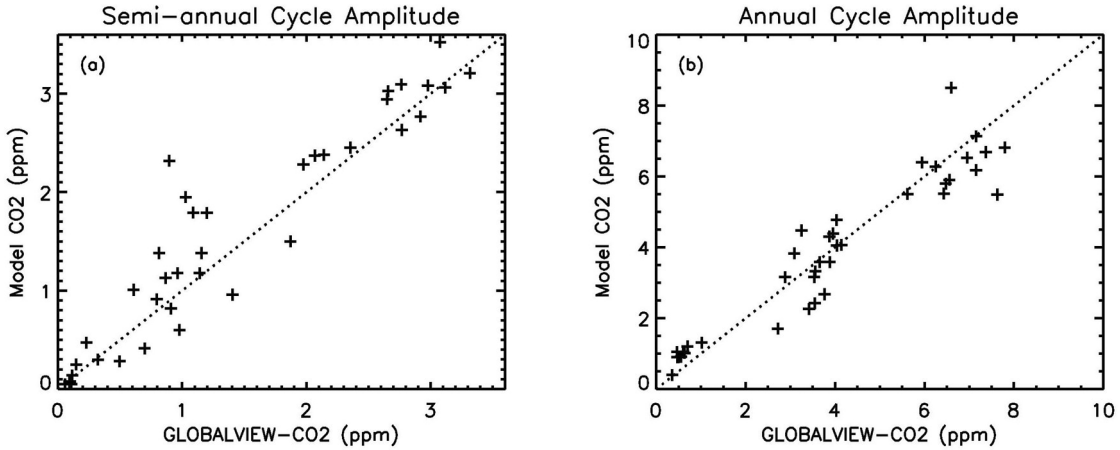


**Figure 5.** (a) Scatterplot of the semiannual cycle amplitude for GLOBALVIEW-$CO_2$ and GEOS-Chem model $CO_2$. (b) Scatterplot of the annual cycle amplitude for GLOBALVIEW-$CO_2$ and GEOS-Chem model $CO_2$.

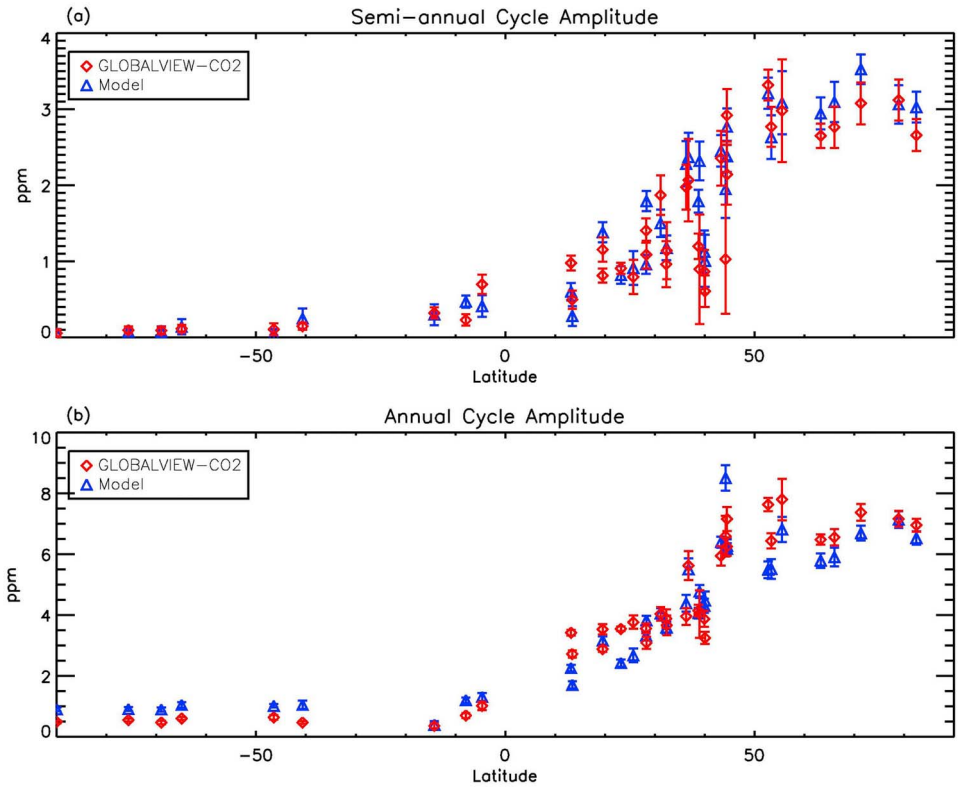


**Figure 6.** (a) Latitudinal distribution of the semiannual cycle amplitude. (b) Latitudinal distribution of the annual cycle amplitude. Diamonds are the results from GLOBALVIEW-$CO_2$. Triangles are the results from the GEOS-Chem model. Error bars are the uncertainties of the results at each latitude band.

latitude, which is consistent from both surface GLOBALVIEW-$CO_2$ data and models. Semiannual and annual cycle amplitudes are larger in the northern hemisphere than in the southern hemisphere. This is because the semiannual and annual cycles in surface $CO_2$ sources (e.g., the net exchange between biosphere and atmosphere) are larger in the northern hemisphere than those in the southern hemisphere.

[16] To investigate possible causes for the semiannual oscillation of $CO_2$ at the surface, we examine the signals from different $CO_2$ surface sources, which include biomass burning, fossil fuel emission, ocean, and biosphere. Fossil fuel emission contributes to the positive trend in $CO_2$. $CO_2$ semiannual cycle and annual cycle are mainly from exchange between the atmosphere and the biosphere. Biomass burning also contributes to the semiannual cycle of $CO_2$. In the current model, the $CO_2$ flux from ocean is an annual mean data. When we have better $CO_2$ fluxes from ocean in the future, we can explore the SAO signal from the ocean in an independent paper. Gross primary production, respiration, and net ecosystem production at 30°N and 110°E, shown in Figure 7, are an example to illustrate the semiannual oscillation in $CO_2$ source from the biosphere. Gross primary production (Figure 7a) is related to carbon uptake by plants during photosynthesis. The values are negative since $CO_2$ is taken up by vegetation from the atmosphere. Ecosystem respiration (Figure 7b) is related to the autotrophic and heterotrophic respirations from biosphere. In the winter season, photosynthesis is largely reduced. The peak for gross primary production (Figure 7a) is relatively flat in winter. However, there are still $CO_2$ emitted to the atmosphere by respirations from the biosphere in winter, which has a relatively sharp peak compared with the photosynthesis term. The sum of the two terms, gross primary production and ecosystem respiration, leads to the double peaks in each year in the net ecosystem production, as shown in Figure 7c. Thus, phase differences in the gross primary production (photosynthesis) and ecosystem respiration lead to the semiannual oscillation in $CO_2$ at the surface. Surface semiannual oscillation can propagate to the middle troposphere, where it produces the semiannual oscillation in the midtropospheric $CO_2$.

## 4. Conclusions

[17] In addition to the annual cycle, the semiannual oscillation of midtropospheric and surface $CO_2$ is discussed in this paper by combining the in situ measurements with chemistry transport models. Chemistry and transport models, driven by different transport schemes, are used to simulate the middle tropospheric $CO_2$. We also apply different boundary conditions to force the 3-D CTMs. The seasonal cycle and semiannual oscillation of surface $CO_2$ are well simulated by chemistry transport model with the prescribed $CO_2$ sources and sinks boundary condition. The semiannual oscillation is also found in the midtropospheric $CO_2$. From the sensitivity study, we found that the semiannual

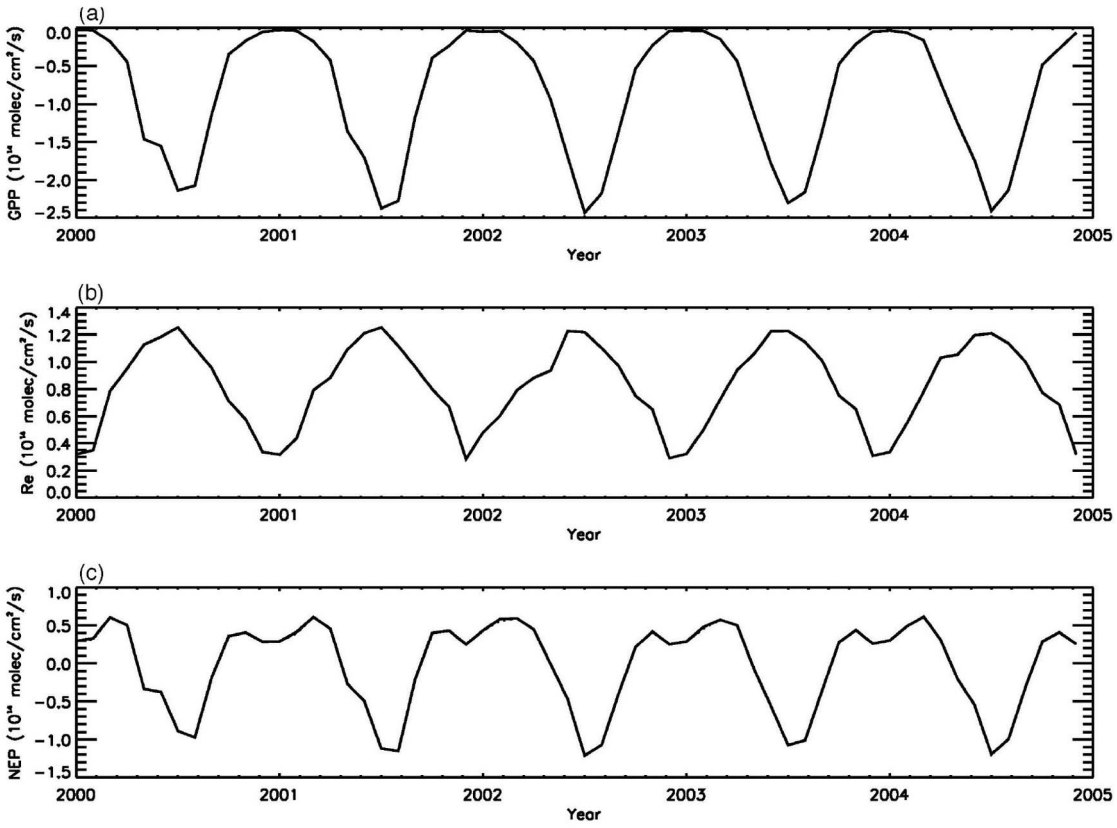


**Figure 7.** (a) Gross primary production, (b) ecosystem respiration, and (c) net ecosystem production from the Carnegie-Ames-Stanford (CASA) ecosystem model at 30°N and 110°E.

oscillation in the midtropospheric $CO_2$ originates mainly from sources at the surface. A possible reason for the semiannual oscillation of surface $CO_2$ is the $CO_2$ surface source due to net ecosystem production.

[18] **Acknowledgments.** We thank two anonymous reviewers and the Associate Editor for the helpful comments. X. Jiang is supported by JPL grant G99694. M. Liang is supported by NSC grant 98-2111-M-001-014-MY3 to Academia Sinica. Y. L. Yung is supported by JPL grant P765982 to the California Institute of Technology.

## References

Allen, D. J., R. B. Rood, A. M. Thompson, and R. D. Hudson (1996a), Three-dimensional radon 222 calculations using assimilated meteorological data and a convective mixing algorithm, *J. Geophys. Res.*, *101*, 6871–6881, doi:10.1029/95JD03408.

Allen, D. J., P. Kasibhatla, A. M. Thompson, R. B. Rood, B. G. Doddridge, K. E. Pickering, R. D. Hudson, and S.-J. Lin (1996b), Transport-induced interannual variability of carbon monoxide determined using a chemistry and transport model, *J. Geophys. Res.*, *101*, 28,655–28,669, doi:10.1029/96JD02984.

Bloom, S., et al. (2005), Documentation and validation of the Goddard Earth Observing System (GEOS) data assimilation system—Version 4, *NASA/TM-2005-104606*, 166 pp., Goddard Space Flight Cent., NASA, Greenbelt, Md.

Buermann, W., et al. (2007), The changing carbon cycle at Mauna Loa Observatory, *Proc. Natl. Acad. Sci. U. S. A.*, *104*, 4249–4254, doi:10.1073/pnas.0611224104.

Dickinson, R. E., and R. J. Cicerone (1986), Future global warming from atmospheric trace gases, *Nature*, *319*(6049), 109–115, doi:10.1038/319109a0.

Duncan, B. N., R. V. Martin, A. C. Staudt, R. Yevich, and J. A. Logan (2003), Interannual and seasonal variability of biomass burning emissions constrained by satellite observations, *J. Geophys. Res.*, *108*(D2), 4100, doi:10.1029/2002JD002378.

Earth System Research Laboratory (ESRL) (2007), *GLOBALVIEW-CO2: Cooperative Atmospheric Data Integration Project—Carbon Dioxide* [CD-ROM], NOAA, Boulder, Colo.

Feng, L., et al. (2011), Evaluating a 3-D transport model of atmospheric $CO_2$ using ground-based, aircraft, and space-borne data, *Atmos. Chem. Phys.*, *11*, 2789–2803, doi:10.5194/acp-11-2789-2011.

Horowitz, L. W., et al. (2003), A global simulation of tropospheric ozone and related tracers: Description and evaluation of MOZART, version 2, *J. Geophys. Res.*, *108*(D24), 4784, doi:10.1029/2002JD002853.

Jiang, X., C. D. Camp, R. Shia, D. Noone, C. Walker, and Y. L. Yung (2004), Quasi-biennial oscillation and quasi-biennial oscillation–annual beat in the tropical total column ozone: A two-dimensional model simulation, *J. Geophys. Res.*, *109*, D16305, doi:10.1029/2003JD004377.

Jiang, X., Q. Li, M.-C. Liang, R.-L. Shia, M. T. Chahine, E. T. Olsen, L. L. Chen, and Y. L. Yung (2008), Simulation of upper tropospheric $CO_2$ from chemistry and transport models, *Global Biogeochem. Cycles*, *22*, GB4025, doi:10.1029/2007GB003049.

Jiang, X., M. T. Chahine, E. T. Olsen, L. L. Chen, and Y. L. Yung (2010), Interannual variability of mid-tropospheric $CO_2$ from Atmospheric Infrared Sounder, *Geophys. Res. Lett.*, *37*, L13801, doi:10.1029/2010GL042823.

Jones, C. D., M. Collins, P. M. Cox, and S. A. Spall (2001), The carbon cycle response to ENSO: A coupled climate–carbon cycle model study, *J. Clim.*, *14*, 4113–4129, doi:10.1175/1520-0442(2001)014<4113:TCCRTE>2.0.CO;2.

Kalnay, E., et al. (1996), The NCEP/NCAR 40-year reanalysis project, *Bull. Am. Meteorol. Soc.*, *77*, 437–471, doi:10.1175/1520-0477(1996)077<0437:TNYRP>2.0.CO;2.

Keeling, C. D., T. P. Whorf, M. Wahlen, and J. Van der Plichtt (1995), Interannual extremes in the rate of rise of atmospheric carbon dioxide since 1980, *Nature*, *375*, 666–670, doi:10.1038/375666a0.

Li, K.-F., B. Tian, D. E. Waliser, and Y. L. Yung (2010), Tropical mid-tropospheric $CO_2$ variability driven by the Madden-Julian oscillation, *Proc. Natl. Acad. Sci. U. S. A.*, *107*, 19,171–19,175, doi:10.1073/pnas.1008222107.

Lin, S.-J., and R. B. Rood (1996), Multidimensional flux-form semi-Lagrangian transport schemes, *Mon. Weather Rev.*, *124*, 2046–2070, doi:10.1175/1520-0493(1996)124<2046:MFFSLT>2.0.CO;2.

Matsueda, H., H. Y. Inoue, and M. Ishii (2002), Aircraft observation of carbon dioxide at 8–13 km altitude over the western Pacific from 1993 to 1999, *Tellus, Ser. B*, *54*(1), 1–21.

Morgan, C. G., M. Allen, M. C. Liang, R. L. Shia, G. A. Blake, and Y. L. Yung (2004), Isotopic fractionation of nitrous oxide in the stratosphere: Comparison between model and observations, *J. Geophys. Res.*, *109*, D04305, doi:10.1029/2003JD003402.

Nevison, C. D., N. M. Mahowald, S. C. Doney, I. D. Lima, G. R. van der Werf, J. T. Randerson, D. F. Baker, P. Kasibhatla, and G. A. McKinley (2008), Contribution of ocean, fossil fuel, land biosphere, and biomass burning carbon fluxes to seasonal and interannual variability in atmospheric $CO_2$, *J. Geophys. Res.*, *113*, G01010, doi:10.1029/2007JG000408.

Randerson, J. T., M. V. Thompson, T. J. Conway, I. Y. Fung, and C. B. Field (1997), The contribution of terrestrial sources and sinks to trends in the seasonal cycle of atmospheric carbon dioxide, *Global Biogeochem. Cycles*, *11*, 535–560, doi:10.1029/97GB02268.

Shia, R.-L., M.-C. Liang, C. E. Miller, and Y. L. Yung (2006), $CO_2$ in the upper troposphere: Influence of stratosphere-troposphere exchange, *Geophys. Res. Lett.*, *33*, L14814, doi:10.1029/2006GL026141.

Suntharalingam, P., C. M. Spivakovsky, J. A. Logan, and M. B. McElroy (2003), Estimating the distribution of terrestrial $CO_2$ sources and sinks from atmospheric measurements: Sensitivity to configuration of the observation network, *J. Geophys. Res.*, *108*(D15), 4452, doi:10.1029/2002JD002207.

Suntharalingam, P., D. J. Jacob, P. I. Palmer, J. A. Logan, R. M. Yantosca, Y. Xiao, M. J. Evans, D. G. Streets, S. L. Vay, and G. W. Sachse (2004), Improved quantification of Chinese carbon fluxes using $CO_2$/CO correlations in Asian outflow, *J. Geophys. Res.*, *109*, D18S18, doi:10.1029/2003JD004362.

Takahashi, T., et al. (1997), Global air-sea flux of $CO_2$: An estimate based on measurements of sea-air $pCO_2$ difference, *Proc. Natl. Acad. Sci. U. S. A.*, *94*, 8292–8299, doi:10.1073/pnas.94.16.8292.

Tans, P. P., et al. (Eds.) (1998), Carbon cycle, in *Climate Monitoring and Diagnostics Laboratory, Summary Rep. 24*, pp. 30–51, Environ. Res. Lab., NOAA, Boulder, Colo.